ELSEVIER

Cross-sectional and longitudinal assessment of the upper cervical spinal cord in motor neuron disease

Hannelore K. van der Burgh[a], Henk-Jan Westeneng[a], Jil M. Meier[a], Michael A. van Es[a], Jan H. Veldink[a], Jeroen Hendrikse[b], Martijn P. van den Heuvel[c,1], Leonard H. van den Berg[a,*,1]

[a] Department of Neurology, UMC Utrecht Brain Center, University Medical Center Utrecht, Utrecht, The Netherlands
[b] Department of Radiology, UMC Utrecht Brain Center, University Medical Center Utrecht, Utrecht, The Netherlands
[c] Department of Complex Trait Genetics, Center for Neurogenomics and Cognitive Research, VU University Amsterdam, Amsterdam, The Netherlands

ABSTRACT

Background: Amyotrophic lateral sclerosis (ALS) is a progressive neuromuscular disease characterized by both upper and lower motor neuron degeneration. While neuroimaging studies of the brain can detect upper motor neuron degeneration, these brain MRI scans also include the upper part of the cervical spinal cord, which offers the possibility to expand the focus also towards lower motor neuron degeneration. Here, we set out to investigate cross-sectional and longitudinal disease effects in the upper cervical spinal cord in patients with ALS, progressive muscular atrophy (PMA: primarily lower motor neuron involvement) and primary lateral sclerosis (PLS: primarily upper motor neuron involvement), and their relation to disease severity and grey and white matter brain measurements.

Methods: We enrolled 108 ALS patients without *C9orf72* repeat expansion (ALS C9–), 26 ALS patients with *C9orf72* repeat expansion (ALS C9 +), 28 PLS patients, 56 PMA patients and 114 controls. During up to five visits, longitudinal T1-weighted brain MRI data were acquired and used to segment the upper cervical spinal cord (UCSC, up to C3) and individual cervical segments (C1 to C4) to calculate cross-sectional areas (CSA). Using linear (mixed-effects) models, the CSA differences were assessed between groups and correlated with disease severity. Furthermore, a relationship between CSA and brain measurements was examined in terms of cortical thickness of the precentral gyrus and white matter integrity of the corticospinal tract.

Results: Compared to controls, CSAs at baseline showed significantly thinner UCSC in all groups in the MND spectrum. Over time, ALS C9– patients demonstrated significant thinning of the UCSC and, more specifically, of segment C3 compared to controls. Progressive thinning over time was also observed in C1 of PMA patients, while ALS C9 + and PLS patients did not show any longitudinal changes. Longitudinal spinal cord measurements showed a significant relationship with disease severity and we found a significant correlation between spinal cord and motor cortex thickness or corticospinal tract integrity for PLS and PMA, but not for ALS patients.

Discussion: Our findings demonstrate atrophy of the upper cervical spinal cord in the motor neuron disease spectrum, which was progressive over time for all but PLS patients. Cervical spinal cord imaging in ALS seems to capture different disease effects than brain neuroimaging. Atrophy of the cervical spinal cord is therefore a promising additional biomarker for both diagnosis and disease progression and could help in the monitoring of treatment effects in future clinical trials.

1. Introduction

Amyotrophic lateral sclerosis (ALS) is a progressive neuromuscular disease, resulting in upper and lower motor neuron degeneration. It is a heterogeneous disease in terms of disease onset and disease progression

(Chiò et al., 2011; Ravits and La Spada, 2009) with a median survival time of 3 years after onset of symptoms (Westeneng et al., 2018). Most in vivo neuroimaging studies in ALS have focused on the brain, showing cortical thinning in several regions including the motor cortex (Agosta et al., 2012; Bede and Hardiman, 2018; Walhout et al., 2015;

Westeneng et al., 2015) and loss of white matter integrity in the structural brain networks of patients with ALS compared to controls (Buchanan et al., 2015; Keil et al., 2012; Schmidt et al., 2014; Verstraete et al., 2011, 2014). Furthermore, a different pattern of brain involvement is demonstrated in a subgroup of patients with a *C9orf72* mutation (Floeter et al., 2016; Westeneng et al., 2016).

Neuroimaging of the brain, however, targets to find upper motor neuron degeneration. Expanding the focus to spinal cord imaging provides an opportunity to investigate not only upper but also lower motor degeneration (El Mendili et al., 2014, 2019). In recent years, spinal cord imaging in ALS has gained more interest (Agosta et al., 2009; Branco et al., 2014; Cohen-Adad et al., 2013; de Albuquerque et al., 2017; El Mendili et al., 2014; Olney et al., 2018; Querin et al., 2017, 2018; Rasoanandrianina et al., 2017; Sperfeld et al., 2005; Valsasina et al., 2007; Wang et al., 2014). While significant atrophy of spinal cord was found in patients with ALS compared to controls, it remains unclear whether thinning occurs throughout the motor neuron disease (MND) spectrum or only in ALS, whether thinning differs according to site-of-onset type, and what is the relationship between thinning and grey and white matter degeneration in the brain.

Brain MRI scans include the upper part of the cervical spinal cord allowing us to investigate the effects of motor neuron loss in this area and also enables to link disease effects on cervical cord MRI to those of the brain. Together with ALS, patients with primary lateral sclerosis (PLS), a primarily upper motor neuron disorder, and progressive muscular atrophy (PMA), a primarily lower motor neuron disorder, make up the MND spectrum and studying these patient groups could therefore help in the identification of the type of motor neuron degeneration driving cervical spinal cord thinning. Moreover, spinal cord imaging might help in characterizing disease effects outside the brain, finding relationships with phenotype, genotype and disease severity, and as a diagnostic and prognostic biomarker. Finally, longitudinal neuroimaging studies have the potential to monitor disease progression and could be used as biomarker in clinical trials.

In the present study, we investigated cross-sectional and longitudinal disease effects in a large cohort of patients with ALS, PLS or PMA using neuroimaging of the upper cervical spinal cord derived from brain MRI.

2. Materials and methods

2.1. Participants

Patients with a MND were recruited from a population-based cohort shortly after diagnosis (Huisman et al., 2011), between 2009 and 2018. ALS patients were diagnosed according to the El Escorial criteria (Brooks et al., 2009). PLS patients were diagnosed according to the Gordon criteria, where the patient fulfilled the criteria at baseline or during follow-up (de Vries et al., 2018; Gordon et al., 2006). For the latter, earlier scans were included in the analyses. Similarly, patients with PMA satisfied previously described criteria from literature (de Vries et al., 2018; Visser et al., 2007). Clinical characteristics such as site of and age at disease onset, and the revised ALS functional rating scale (ALSFRS-R) score as measure for disability (Cedarbaum et al., 1999) were recorded. The same protocol was used to acquire longitudinal data. Genomic DNA samples of patients were screened for the *C9orf72* repeat expansion, using a repeat primed PCR as previously described (Van Rheenen et al., 2012). Patients have not been screened routinely for other ALS-related mutations as these are relatively rare. Patients had no history of brain injury, psychiatric illness, epilepsy, or neurodegenerative diseases other than ALS or frontotemporal dementia. Control subjects were also selected from a Dutch population-
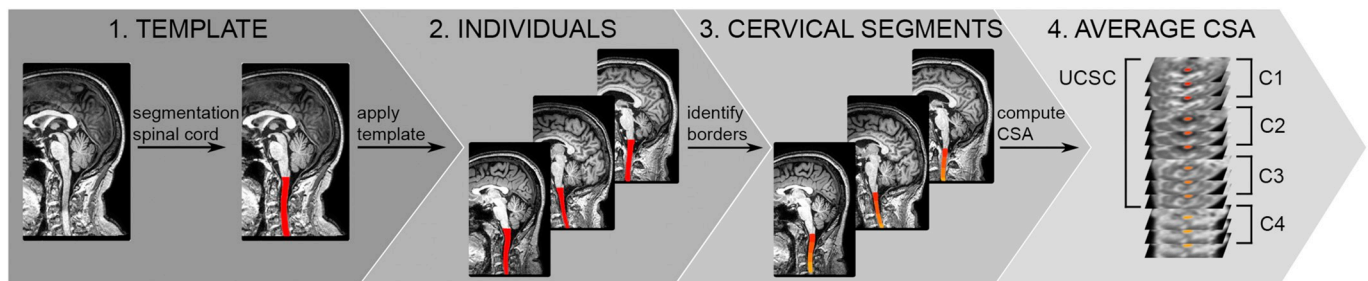

Fig. 1. Cervical spinal cord segmentation. 1) A control subject was appointed as template for spinal cord segmentation. 2) The initial segmenting starting point derived on the template was brought to individual space and used to segment the spinal cord of each subject. 3) For each subject, borders of the cervical spinal cord segments were identified as the center of intervertebral disks. 4) The cross-sectional area (CSA) of each segmentation slice was computed and averaged over the first three cervical segments (UCSC) or for individual segments (C1–C4).

Table 1
Demographic and clinical characteristics of all study participants at baseline.

	ALS C9−	ALS C9+	PLS	PMA	CON	p-value
n (n follow-up)	108 (64)	26 (18)	28 (18)	56 (41)	114 (54)	
Follow-up interval, m (median, range)	4.9[c] (3.0–9.8)	5.4[c] (3.0–10.0)	6.8[c] (3.2–85.9)	5.5[c] (3.0–59.0)	14.7 (4.3–50.8)	0.009
Gender (%)						0.007
Male	59 (54.6)	17 (65.4)	17 (60.7)	46 (82.1)	63 (55.3)	
Female	49 (45.4)	9 (34.6)	11 (39.3)	10 (17.9)	51 (44.7)	
Age at 1st MRI (median, range)	64.6 (30.6–80.5)	59.7 (40.6–67.0)	60.2 (36.1–78.3)	63.1 (22.6–80.1)	65.0 (30.8–79.4)	0.027
Site of onset (%)						< 0.001
Bulbar	30 (27.8)	5 (19.2)	3 (10.7)	0 (0.0)	–	
Spinal	78 (72.2)	21 (80.8)	25 (89.3)	56 (100)	–	
Disease duration[a,b] (median, range)	14.4 (2.9–174.4)	11.5 (3.3–68.3)	90.6 (23.5–224.9)	20.3 (4.6–467.4)	–	< 0.001
ALSFRS-R score (median, range)	40 (23–47)	41 (30–47)	39 (28–44)	41.5 (25–48)	–	0.027

[a] Disease duration was measured from disease onset until date of the first MRI in months.

[b] Diagnosis of PLS and PMA was given after 4 years, but prior (baseline) scans were included in analyses.

[c] Denotes characteristics that significantly differ (p < .05) between a patient group and their matched control group. The column of p-values denotes significant differences between the patient groups.
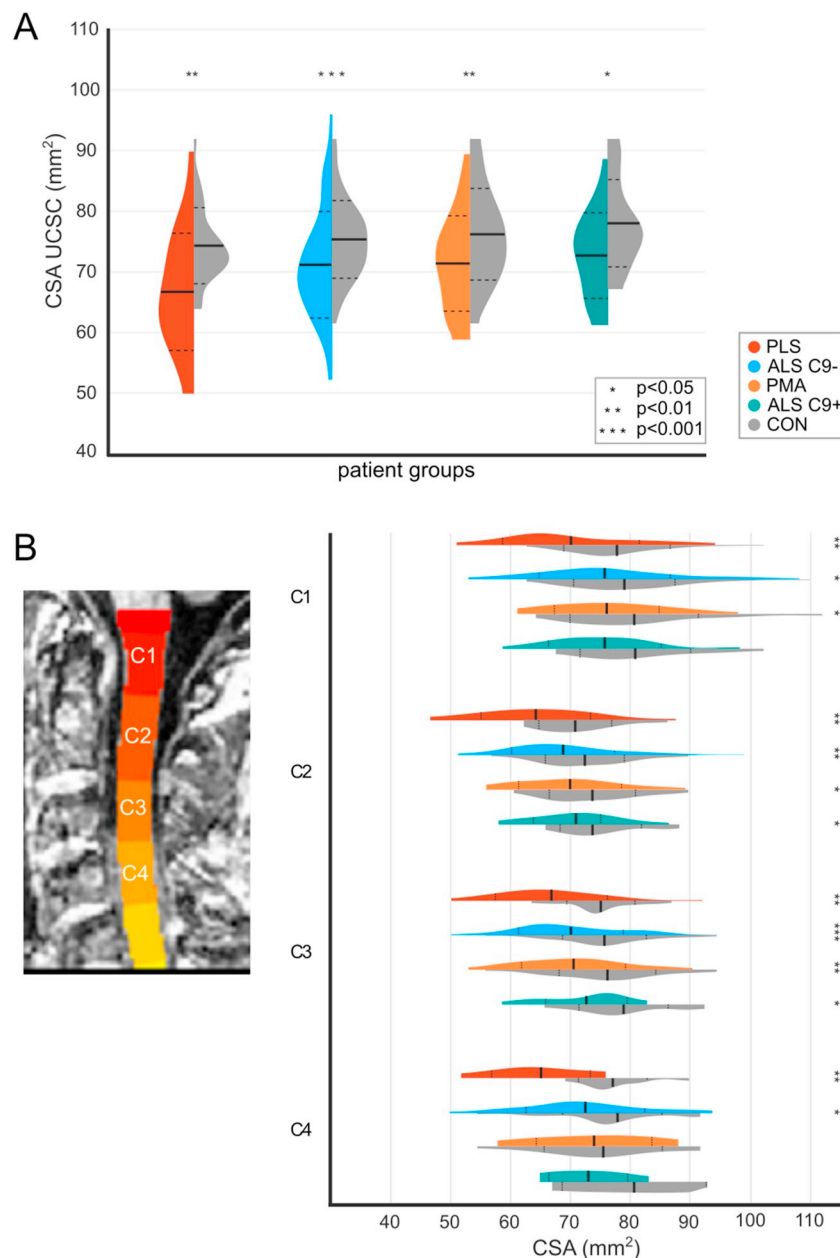
Fig. 2. CSA of UCSC and individual segments. A) The CSA of UCSC for each patient group (PLS, ALS C9–, PMA and ALS C9+) was compared to their age- and gender-matched controls (CON). Solid lines denote the mean CSA and dashed lines reflect the mean ± standard deviation boundaries. B) Comparison between patient and control groups for cervical segments C1–C4.

based cohort (Huisman et al., 2011). These controls are, therefore, not necessarily healthy but are controls in the sense that they have no MND or a history of brain injury, psychiatric illness or epilepsy. Participants (patients and controls) with cervical myelopathy, cervical radiculopathy, spinal trauma or spinal surgery of the studied spinal segments, and subjects with demyelinating conditions (multiple sclerosis / neuromyelitis optica) were also excluded. The Ethical Committee for human research of the University Medical Center Utrecht approved the study protocols and informed written consent, according to the Declaration of Helsinki, was obtained from each subject.

2.2. Image acquisition

From all subjects, T1 scans were acquired using a 3 Tesla Philips Achieva Medical Scanner with a SENSE receiver head-coil, initially for the purpose of brain imaging. Each high-resolution T1-weighted image was

acquired by a 3D fast field echo using parallel imaging (acquisition time = 11 min, TR/TE = 10/4.6 ms, flip-angle 8°, slice orientation: sagittal, voxel size = 0.80 × 0.75 × 0.75 mm, field of view (FOV) = 176 × 240 × 240 mm, gradient nonlinearity correction was applied), covering the whole brain and the first segments of the cervical spinal cord (C1-C2). The proportion of other cervical spinal cord segments (C3-C5) present on the images depended on the subject's head size and position in the field of view, while the subject's head and upper cervical spinal cord (UCSC) was consistently positioned in the middle of the head coil.

Furthermore, diffusion-weighted images (DWI) of the brain were acquired to assess white matter. For this, two sets of 30 diffusion-weighted scans and five unweighted B0 scans each were acquired as follows: DWI-MR using parallel imaging SENSE, p-reduction = 3, gradient set of 30 different weighted directions, b = 1000 s/mm^2, TR/TE = 7035/68 ms, 2 × 2 × 2 mm voxel size, 75 slices, second set with reversed k-space read-out, acquisition time = 4.5 min.

Table 2
Cross-sectional CSA results for ALS, PLS, PMA and their matched controls.

		CSA PAT	CSA CON	ΔCSA	p-value	FDR-corrected p-value
ALS C9–	UCSC	71.03 ± 7.55	75.30 ± 7.55	4.27	< 0.001	< 0.001
	C1	75.41 ± 9.62	78.75 ± 9.62	3.34	**0.010**	**0.016**
	C2	68.51 ± 7.41	72.22 ± 7.41	3.71	< 0.001	**0.001**
	C3	69.87 ± 7.79	75.53 ± 7.79	5.66	< 0.001	< 0.001
	C4	72.57 ± 9.26	76.87 ± 9.21	4.30	**0.025**	**0.030**
ALS C9 +	UCSC	72.36 ± 6.96	77.31 ± 7.11	4.77	**0.019**	**0.030**
	C1	74.72 ± 9.42	79.75 ± 9.68	4.90	0.052	0.066
	C2	70.11 ± 6.96	74.28 ± 7.15	3.98	**0.032**	**0.047**
	C3	72.25 ± 7.19	78.15 ± 7.54	5.73	**0.006**	**0.013**
	C4	73.19 ± 10.69	80.43 ± 9.95	7.23	0.301	0.309
PLS	UCSC	66.89 ± 7.16	73.55 ± 7.26	6.66	**0.003**	**0.005**
	C1	69.14 ± 9.34	76.73 ± 9.34	7.59	**0.003**	**0.005**
	C2	63.47 ± 7.22	70.01 ± 7.21	6.54	< 0.001	**0.002**
	C3	66.89 ± 6.98	74.32 ± 7.07	7.43	< 0.001	**0.003**
	C4	65.50 ± 7.02	77.99 ± 7.80	12.49	**0.002**	**0.005**
PMA	UCSC	71.17 ± 8.42	75.80 ± 8.79	4.64	**0.002**	**0.005**
	C1	74.24 ± 11.14	78.83 ± 11.14	4.59	**0.011**	**0.016**
	C2	69.43 ± 8.99	73.16 ± 8.99	3.74	**0.011**	**0.016**
	C3	70.82 ± 8.98	76.30 ± 9.37	5.48	< 0.001	**0.002**
	C4	74.64 ± 9.69	75.15 ± 10.03	0.52	0.876	0.876

CSA PAT and CSA CON are the estimated marginal means, corrected for age and gender (in mean ± standard deviation). All CSA values are in mm^2.
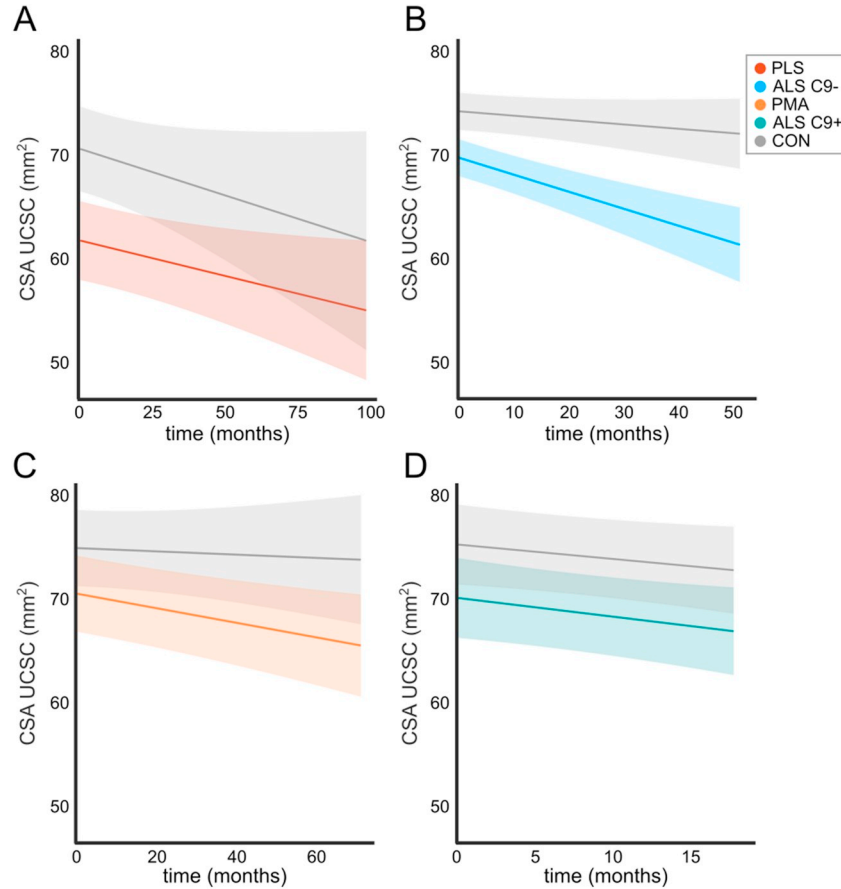P-values < 0.05 are denoted in bold.

Fig. 3. Estimates of longitudinal CSA change. A) PLS patients compared to their matched controls. B) ALS C9– patients compared to their matched controls. C) PMA patients compared to their matched controls. D). ALS C9 + patients compared to their matched controls (CON).

2.3. Spinal cord data processing

Using the T1-weighted images, we identified a control subject with minimal anterior-posterior and left-right curvature of the spine and the most cervical segments (C1-C5). This subject was set to be the experimental standard template, following the framework of Kong et al. (2014).

The spinal cord of the template was segmented, using segmentation functions of the Spinal Cord Toolbox (De Leener et al., 2017), by manually setting the initial segmenting starting point for the template (Fig. 1).

The T1-weighted image of each subject was registered to the template by applying FSL's non-linear image registration algorithm (FNIRT), which used the output of the linear registration algorithm

Table 3
Longitudinal CSA reduction (ΔCSA, in mm²/month) for the ALS, PLS and PMA groups compared to their matched controls.

		ΔCSA	p-value	FDR-corrected p-value
ALS C9–	UCSC	0.004	**0.006**	**0.046**
	C1	0.003	0.125	0.297
	C2	0.004	**0.021**	0.093
	C3	0.005	**0.003**	**0.044**
	C4	< 0.001	0.994	0.999
ALS C9 +	UCSC	0.001	0.771	0.999
	C1	0.003	0.169	0.377
	C2	0.004	0.611	0.989
	C3	0.001	0.876	0.999
	C4	0.007	0.518	0.893
PLS	UCSC	< 0.001	0.999	0.999
	C1	0.001	0.407	0.744
	C2	< 0.001	0.999	0.999
	C3	0.002	0.998	0.999
	C4	0.006	**0.022**	0.097
PMA	UCSC	0.002	0.062	0.206
	C1	0.004	**0.006**	**0.048**
	C2	0.001	0.968	0.999
	C3	0.003	0.078	0.230
	C4	0.004	0.091	0.261

(FLIRT) as affine starting guess. From this registration, an inverse transform matrix was obtained, which, in turn, was applied to bring the segmentation starting point of the template to individual subject space. Next, the spinal cord of all subjects was segmented using the Spinal Cord Toolbox based on the derived initial starting point as input in order to optimize the performance of these segmentation functions. Each segmentation was visually checked and, if necessary, improved manually (blinded for disease status). Finally, the centers of intervertebral disks served as the borders dividing the cervical spinal cord segments and were identified for all subjects (Fig. 1).

2.4. Brain data processing

Cortical and subcortical brain regions were analyzed using T1 images and FreeSurfer (V5.3.0, http://surfer.nmr.mgh.harvard.edu/). In total, 83 distinct brain regions (68 cortical regions, 14 subcortical regions and brainstem) were parcellated and segmented (Fischl et al., 2002, 2004) according to the Desikan-Killiany atlas (Desikan et al., 2006). From the DWI dataset, white matter integrity was assessed. Preprocessing included correction for susceptibility and eddy-current distortions, as previously described (Verstraete et al., 2011). Next, the images were processed with the TRACULA tool (TRActs Constrained by Underlying Anatomy) for automated reconstruction of major white matter tracts, like the corticospinal tract (CST), using global probabilistic tractography (Yendiki et al., 2011). The output included fractional anisotropy (FA), radial diffusivity (RD) and mean diffusivity (MD) values for the major white matter tracts.

2.5. Cross-sectional area

We calculated the mean cross-sectional area (CSA) of the upper cervical spinal cord (UCSC), defined as the mean of all slices in the first three spinal cord segments (i.e. C1–C3, Fig. 1) with CSA of each segmentation slice computed using the *sct_process_segmentation* function of the Spinal Cord Toolbox (De Leener et al., 2017). This function counts pixels in each slice, multiplies them by the voxel area and then geometrically adjusts this using the centerline orientation of the spinal cord to obtain the CSA. Next, we investigated disease effects in individual cervical segments, defined by the identified borders, and computed the mean CSA over all slices in each segment (Fig. 1). For this analysis, we also included segment C4 as the CSA in this segment could be calculated

for at least 25% of subjects in each patient group. In contrast, C5 was usually (90%) outside the field of view, so we constrained the segment-wise comparison to C1–C4.

2.6. Statistical analysis

Statistical analyses were executed using MATLAB Release 2017b, including the Statistics Toolbox (The MathWorks, Inc., Natick, Massachusetts, United States; http://www.mathworks.com). We matched each patient to an age- and gender-matched control subject. For this, we first divided the patient and control groups according to gender. For each gender-group, we then calculated the Euclidean distance based on age between each patient and the controls. The control subject with the smallest distance was chosen as the match for this patient and was not available anymore for the matching algorithm of this patient subgroup.

First, baseline cross-sectional analyses were performed. Patient groups were compared to their age- and gender-matched controls based on their upper spinal cord and segment-wise measurements. No direct comparisons between patient subgroups were performed due to the dependence of disease duration, different sample sizes of the groups, and because we focused primarily on 'abnormality' (thus compared to controls). We therefore restricted the analyses to comparisons with age- and gender-matched controls.

Significance between groups was assessed by means of linear models (age and gender were used as covariates) and permutation tests in which group labels were randomly assigned (10,000 permutations). P-values < 0.05, after FDR-correction for multiple testing, were considered statistically significant. We used the algorithm of Benjamini and Hochberg for this FDR-correction (Benjamini and Hochberg, 1995).

Second, we conducted longitudinal analyses using linear mixed-effects models to assess CSA change over time. Age and gender were included as covariates and we accounted for random between-subject variation of slopes and intercepts. To examine disease effects and to compare whether one group shows faster deterioration than others, we included an interaction term (follow-up time × group), where follow-up time was defined as the time since baseline scan at follow-up scan, and group referred to patient or control. The reported values reflect the greater amount of CSA that a patient group has lost per month compared to the control group.

Third, we investigated CSA in relationship to phenotype, where we stratified the *C9orf72*-negative ALS patient group (ALS C9–) for their site of disease onset (bulbar or spinal). Furthermore, the CSAs of patients were correlated with their total ALSFRS-R scores and their total ALSFRS-R minus the bulbar sub-score (spinal ALSFRS-R sub-score (Rasoanandrianina et al., 2017)), obtained at the time of scan, to link the spinal cord measurements to disease severity. For the longitudinal MRI and ALSFRS-R measurements, a linear model with random slopes and intercepts was computed. Finally, we investigated a possible link between brain measurements (i.e. cortical thickness of precentral gyrus and FA of the CST) and CSA.

3. Results

3.1. Participants

In total, 108 ALS C9– patients and 26 ALS patients with a *C9orf72* mutation (ALS C9 +), 28 PLS and 56 PMA patients participated in the study (Table 1 and S1). In addition, 114 unrelated population-based controls were included in the study and matched based on age and gender to each of the patient groups (Table S2). Follow-up data (up to five visits, Table S3) were available for 64 ALS C9–, 18 ALS C9 +, 18 PLS and 41 PMA patients. Of the total control group of 114 subjects, 54 controls had two visits (i.e. 51 controls matched to the ALS C9– group, 11 controls for the ALS C9 + group, 12 controls for the PLS and 25 controls for the PMA patients). CSA of segments C1 and C2 were available for all participants (Table S4). The CSA of C3 and C4 could be calculated for at least 75% and 25% of the participants in each subject group, respectively.
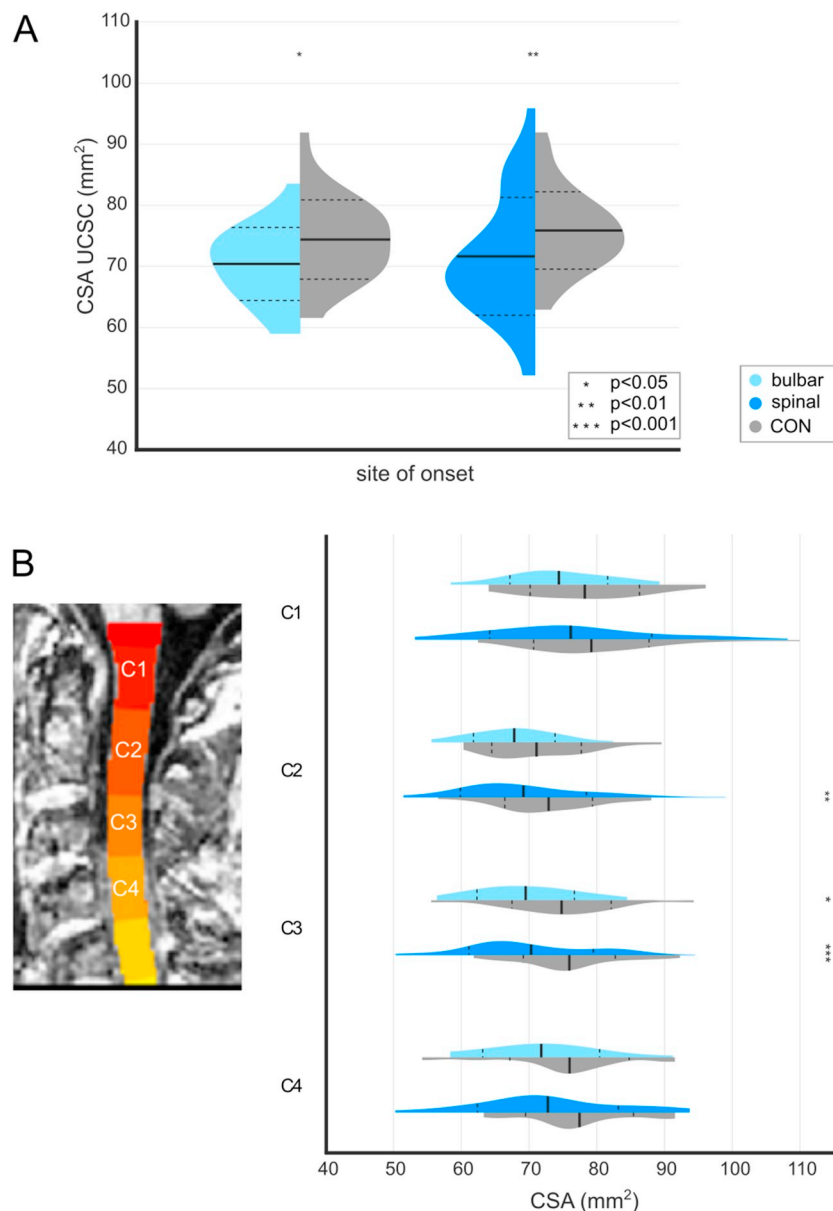
Fig. 4. CSA stratified for site of onset. A) CSA of UCSC for patients with either bulbar or spinal onset compared to their matched controls. B) Comparison at individual cervical segment levels.

3.2. Baseline disease effects

At baseline, ALS C9– patients showed a significantly thinner UCSC CSA than controls (mean estimated difference CSA (ΔCSA) = $-4.27\,\text{mm}^2$, 95%-CI$[-6.27; -2.27]$, p < 0.001, Fig. 2A, Table 2). Compared to controls, a significant thinner UCSC was also observed in PLS (mean ΔCSA = $-6.66\,\text{mm}^2$, 95%-CI$[-10.68; -2.63]$, p = 0.005) and PMA patients (mean ΔCSA = $-4.64\,\text{mm}^2$, 95%-CI$[-7.52; -1.75]$, p = 0.005). Finally, the mean CSA of the UCSC of ALS C9+ was significantly lower compared to controls at baseline (mean ΔCSA = $-4.77\,\text{mm}^2$, 95%-CI $[-8.76; -0.78]$, p = 0.030).

ALS C9– and PLS patients showed differences in CSA compared to their controls for all individual segments of the cervical spinal cord (C1–C4, Fig. 2B, Table 2). The CSA of the PMA group were significantly lower than the controls at level C1–C3. Finally, the ALS C9+ patients displayed thinner segments compared to control at level C2 and C3.

Patients with and without follow-up data displayed similar CSA results at baseline, with no significant difference between the two groups (Fig. S1). Averaging only segments C2 and C3 instead of UCSC

(i.e. C1–C3) resulted in similar findings as for UCSC (Table S5).

3.3. Longitudinal disease effects

Over time, ALS C9– patients revealed significant thinning in the UCSC measurement compared to controls (ALS C9–: mean CSA reduction = $0.004\,\text{mm}^2$/month, 95%-CI$[-0.007; -0.001]$, p = 0.044; Fig. 3). In contrast, the PLS, PMA and ALS C9+ patients showed no significant changes over time (Table 3). Similar findings were observed after averaging only C2 and C3 (Table S6).

Compared to controls, significant thinning of C3 was observed over time in ALS C9– patients, but no longitudinal changes in segments C1, C2 and C4 (Table 3). Progressive thinning over time was also observed in C1 of PMA patients, whereas the spinal cord thickness of the PLS and ALS C9+ group did not change over time in any of the examined segments.

3.4. Relationship with site of onset

In ALS C9– patients, both the bulbar- (n = 30) and spinal-onset

Table 4
Cross-sectional CSA comparison between bulbar and spinal onset ALS C9– patients and controls.

		CSA PAT	CSA CON	ΔCSA	p-value	FDR-corrected p-value
Bulbar	UCSC	70.24 ± 6.16	74.36 ± 6.16	4.12	**0.011**	**0.022**
	C1	74.25 ± 7.72	78.18 ± 7.72	3.93	0.056	0.077
	C2	67.61 ± 6.19	71.05 ± 6.20	3.43	**0.032**	0.054
	C3	69.39 ± 7.18	74.84 ± 7.18	5.45	**0.004**	**0.010**
	C4	71.66 ± 8.23	74.87 ± 8.39	3.21	0.280	0.281
Spinal	UCSC	71.32 ± 8.02	75.66 ± 8.02	4.33	**< 0.001**	**0.003**
	C1	75.84 ± 10.30	78.96 ± 10.30	3.12	0.062	0.077
	C2	68.84 ± 7.83	72.66 ± 7.83	3.82	**0.002**	**0.007**
	C3	70.04 ± 8.02	75.78 ± 8.02	5.74	**< 0.001**	**< 0.001**
	C4	73.47 ± 9.52	77.69 ± 9.31	4.23	0.084	0.093

		CSA BULBAR	CSA SPINAL	ΔCSA	p-value	FDR-corrected p-value
	UCSC	70.51 ± 8.75	71.27 ± 8.74	0.76	0.690	–
	C1	74.51 ± 10.98	75.86 ± 10.97	1.34	0.567	–
	C2	67.93 ± 8.41	68.76 ± 8.40	0.84	0.645	–
	C3	69.64 ± 8.72	69.99 ± 8.70	0.35	0.850	–
	C4	72.75 ± 10.09	73.02 ± 10.12	0.27	0.934	–

Table 5
Longitudinal CSA reduction (ΔCSA, in mm^2/month) for the ALS C9– patients, stratified for site of onset, compared to their matched controls.

		ΔCSA	p-value	FDR-corrected p-value
Bulbar vs CON	UCSC	0.004	0.344	0.746
	C1	0.002	0.739	0.746
	C2	0.001	0.741	0.746
	C3	0.011	**0.048**	0.237
	C4	0.003	0.746	0.746
Spinal vs CON	UCSC	0.004	**0.005**	**0.026**
	C1	0.003	0.122	0.153
	C2	0.005	**0.012**	**0.027**
	C3	0.005	**0.016**	**0.027**
	C4	< 0.001	0.991	0.991
Bulbar vs spinal	UCSC	0.001	0.925	–
	C1	0.002	0.674	–
	C2	0.004	0.893	–
	C3	0.006	0.522	–
	C4	0.001	0.941	–

(n = 78) patients showed a significantly reduced mean UCSC CSA compared to controls (bulbar onset: mean ΔCSA = − 4.12 mm^2, 95%-CI [− 7.19; − 1.04], p = 0.022; spinal onset: mean ΔCSA = − 4.33 mm^2, 95%-CI[− 6.83; − 1.83], p = 0.003; no significant difference was found between the two groups (Fig. 4A and Table 4). Both onset types displayed a significantly smaller mean CSA in segment C3 compared to controls, where spinal-onset patients additionally revealed significantly smaller CSA at the level of C2 (Fig. 4B and Table 4). Again, there were no significant differences between the separate segments when comparing the bulbar and spinal onset groups directly.

Over time, the spinal-onset patients displayed progressive thinning of UCSC (mean ΔCSA = − 0.004 mm^2, 95%-CI[− 0.007; − 0.001], p = 0.026) and, more specifically, of segments C2 and C3 (Table 5). No significant thinning could be revealed for patients with bulbar onset (UCSC: mean ΔCSA = − 0.004 mm^2, 95%-CI[− 0.010; 0.003], p = 0.746) or between the two site-of-onset groups.

3.5. Relationship with ALSFRS-R

The total ALSFRS-R score correlated significantly with the upper spinal cord measurement of PLS patients ($r = 0.557$, p = 0.009, Fig. 5A) and the first three segments separately (C1: $r = 0.547$, p = 0.003; C2: $r = 0.541$, p = 0.003; C3: $r = 0.463$, $p = 0.034$; C4: $r = 0.349$, p = 0.396). Of note, the correlation for C4 was based on only eight subjects, so insufficient power could explain the lack of a significant correlation with the total

ALSFRS-R score in this segment. In the other groups, we observed no significant correlations between the upper spinal cord measurement and the total ALSFRS-R score, nor for the individual segments (Table S7).

Using longitudinal scan data and longitudinal ALSFRS-R total scores, significant correlations were found for PLS ($r = 0.677$, p < 0.001, Fig. 5B, Table S8), ALS C9– ($r = 0.318$, p < 0.001, Fig. 5C) and PMA ($r = 0.233$, p = 0.016, Fig. 5D), suggesting that thinning of the cervical spinal cord is reflected in lowering total scores on the ALSFRS-R and thus increasing disease severity. For ALS C9 + patients, the correlation did not reach significance ($r = 0.316$, p = 0.134, Fig. 5E).

Similar results were found for the spinal ALSFRS-R sub-score in the various groups for both the cross-sectional and longitudinal analyses (Tables S7 and S8).

3.6. Relationship with cerebral motor system

In contrast to the UCSC result, only the ALS C9– and ALS C9 + patients displayed a significantly thinner motor cortex of the precentral gyrus (averaged over both hemispheres, Fig. 6A) compared to their matched controls at group-level. However, correlating CSA with cortical thickness of the precentral gyrus did not reveal a significant relationship (Table 6).

For the cerebral part of corticospinal tract, the ALS C9– patients showed significantly lower FA than their matched controls, whereas the other patient groups did not (Fig. 6B). The MD of the CST was significantly increased for all but PMA patients and we only found significantly increased RD of the CST for ALS C9– (Table S9). The PLS and PMA groups displayed a significant correlation between FA of the CST and CSA, both for UCSC and separate segments, although the direction of the correlation was opposite between these two groups (Table 6). We found similar results when using RD or MD as white matter integrity measure for the CST. Only for ALS C9 +, other major white matter tracts reached significance (Table S9).

4. Discussion

In the present study, we investigated the value of upper cervical spinal cord measurements as biomarker of diagnosis and disease progression in patients with ALS, and its upper motor neuron variant, PLS, and lower motor neuron variant, PMA. We showed a thinner upper cervical spinal cord compared to controls in all disease groups (ALS, PLS and PMA), which might suggest that cervical spinal cord thinning is related to both upper and lower motor neuron loss. Interestingly, patients with a *C9orf72* repeat expansion, who have an MRI phenotype
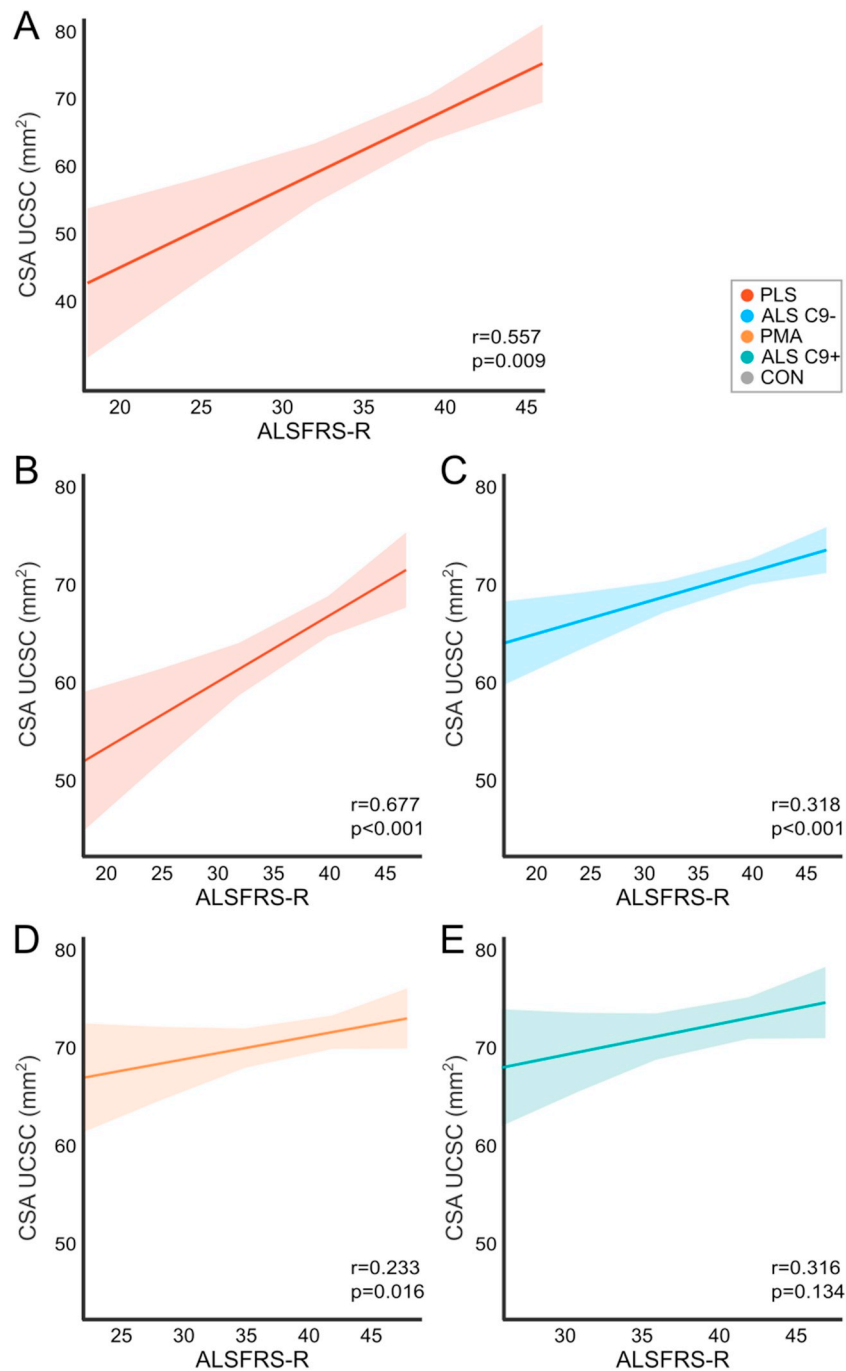
Fig. 5. CSA relationship with ALSFRS-R. A) At baseline, there is a significant positive correlation between the total ALSFRS-R score and CSA of UCSC for PLS patients. B) Estimates of longitudinal CSA change in the UCSC with respect to the total ALSFRS-R score for PLS, C) ALS C9–, D) PMA and E) ALS C9 + .

characterized by widespread cortical thinning (Bede et al., 2013; Westeneng et al., 2016), did not show such widespread significantly thinner cervical spinal cord at baseline. Over time, significant thinning occurred in the ALS patient group without *C9orf72* repeat expansion, while the PMA patients only show thinning in one segment (C1), and ALS C9+ as well as PLS patients displayed no significant longitudinal thinning at all. Longitudinal cervical spinal cord imaging might, therefore, be a valuable biomarker of disease progression in clinical trials.

Several previous studies showed no differences in spinal cord area or diameter between ALS patients and controls at the level of C2-C4 (Sperfeld et al., 2005; Wang et al., 2014). Other research revealed a thinner spinal cord in these regions, applying 1.5 T or 3 T MRI in up to 64 patients (Agosta et al., 2009; Branco et al., 2014; de Albuquerque

et al., 2017; Olney et al., 2018; Rasoanandrianina et al., 2017; Valsasina et al., 2007). Differences in results might be explained by the use of 1.5 T or 3 T MRI scanner, different study population sizes or the measurements of only one slice in a segment, a mid-vertebra slice, or an average over slices in entire segments. Compared to studies that also found thinner spinal cord cross-sectionally, we demonstrated smaller area differences (Branco et al., 2014; de Albuquerque et al., 2017; Olney et al., 2018; Valsasina et al., 2007). Disease duration of the patients at baseline might also influence the CSA differences: the median disease duration of the ALS patients in our population is shorter than in study populations of previous research. Therefore, our cross-sectional findings might reflect an earlier phase of upper cervical spinal cord degeneration since our longitudinal analyses also showed growing
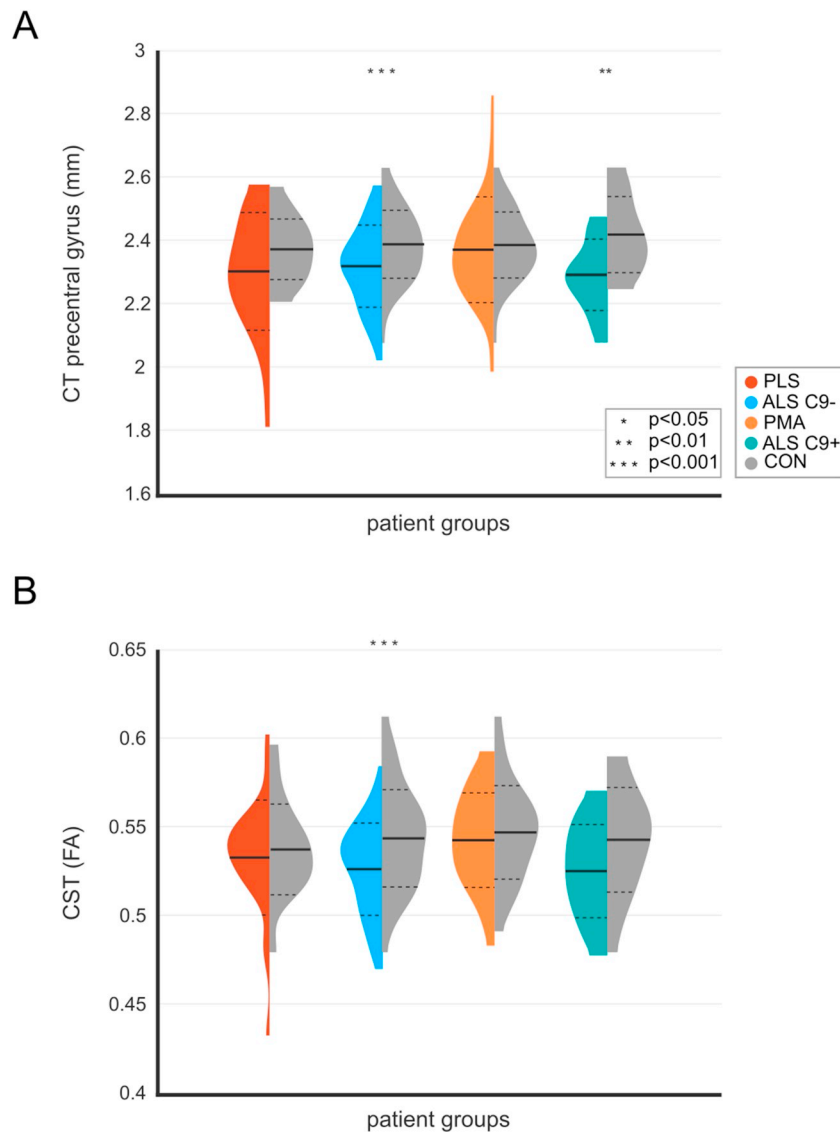
A

B

Fig. 6. Brain measurements. A) Cortical thickness (CT) of the precentral gyrus (both hemispheres averaged). B) Fractional anisotropy (FA) of corticospinal tract (CST).

differences over time. We demonstrated in a large well-characterized, *C9orf72*-genotyped cohort of patients, thinner spinal cord in MND patients, by both examining the mean CSA in UCSC and individual segments. In this way, we obtained a robust measure of spinal cord thickness, while still considering the possibly variable behavior of the disease at different levels of the cervical spinal cord. We anticipate applying these analyses to MRI of the entire spinal cord also including thoracic and lumbosacral segments in future studies.

Over time, we demonstrated thinning of the UCSC in ALS C9– patients, which is in line with previous studies (Agosta et al., 2009; de Albuquerque et al., 2017; El Mendili et al., 2014). We found no significant longitudinal change in the UCSC for the other patient groups. This might be explained by a relatively more substantial decrease of CSA in controls in these groups (reductions of 2.38 mm²/year and 1.54 mm²/year for controls matched to ALS C9 + and PLS, compared to reductions of 1.08 mm²/year and 0.98 mm²/year for controls matched to ALS C9– and PMA). This substantial decrease in controls could be due to smaller group sizes. The similar reduction of the CSA that seems to occur for ALS C9 + and ALS C9– patients supports this explanation. Comparing these decreases of CSA in controls to literature (Casserly et al., 2018; de Albuquerque et al., 2017), they are higher than expected (Fig. S3) and could be caused by our study design: although subjects

with spinal cord diseases were excluded, controls were not necessarily healthy as they were recruited from a population-based cohort to reduce potential selection bias. Overall, the small sample sizes and the noteworthy decrease of CSA in controls might potentially create a bias in the longitudinal results. In specific segments, thinning over time was seen for all patient groups except ALS C9 + and PLS. The absence of significant thinning over time for the PLS group might be explained by the longer disease duration at baseline in these patients. Thinning of upper spinal cord in ALS patients in our study was not driven by site of onset. The smaller group of patients with bulbar onset could explain the absence of significant thinning for this group over time as the slope of CSA reduction per month is similar to the slope in spinal-onset patients. A difference between the site-of-onset groups might be revealed more pronounced when examining lower segments of the (cervical) spinal cord. For example, patients with upper-limb onset seem to have a distinct metabolic activation in cervical segments compared to lower-limbonset patients (Marini et al., 2018).

We could not reveal significant correlations between CSA and the ALSFRS-R total score, with or without bulbar sub-scores, for the ALS patients at baseline, and thus could not demonstrate a significant relationship between spinal cord thickness and functional disability at this time point. Previous results concerning this aspect have been

Table 6
Correlations between CSA and brain measurements (cortical thickness of precentral gyrus and FA of the CST).

		UCSC	C1	C2	C3	C4
Precentral gyrus	ALS C9−	r = 0.158	r = 0.181	r = 0.163	r = 0.101	r = 0.070
		p = 0.103	p = 0.061	p = 0.093	p = 0.297	p = 0.634
	ALS C9 +	r = −0.069	r = −0.193	r = −0.225	r = −0.114	r = −0.196
		p = 0.767	p = 0.346	p = 0.270	p = 0.624	p = 0.674
	PLS	r = 0.294	r = 0.259	r = 0.362	r = 0.291	r = 0.130
		p = 0.208	p = 0.199	p = 0.064	p = 0.213	p = 0.760
	PMA	r = 0.005	r = 0.053	r = 0.014	r = 0.014	r = −0.114
		p = 0.971	p = 0.698	p = 0.916	p = 0.924	p = 0.652
CST	ALS C9−	r = −0.014	r = −0.024	r = −0.013	r = 0.006	r = −0.008
		p = 0.885	p = 0.803	p = 0.893	p = 0.950	p = 0.959
		p_{adj} = 0.959	p_{adj} = 0.959	p_{adj} = 0.959	p_{adj} = 0.959	p_{adj} = 0.959
	ALS C9 +	r = −0.192	r = −0.156	r = −0.071	r = −0.129	r = −0.549
		p = 0.444	p = 0.489	p = 0.754	p = 0.609	p = 0.259
		p_{adj} = 0.740	p_{adj} = 0.752	p_{adj} = 0.959	p_{adj} = 0.871	p_{adj} = 0.518
	PLS	**r = 0.551**	**r = 0.410**	**r = 0.520**	**r = 0.527**	r = 0.697
		p = 0.012	**p = 0.034**	**p = 0.005**	**p = 0.017**	p = 0.082
		p_{adj} = 0.039	**p_{adj} = 0.042**	**p_{adj} = 0.032**	**p_{adj} = 0.039**	p_{adj} = 0.091
	PMA	**r = −0.358**	**r = −0.321**	**r = −0.388**	**r = −0.349**	r = −0.223
		p = 0.023	**p = 0.026**	**p = 0.006**	**p = 0.027**	p = 0.391
		p_{adj} = 0.039	**p_{adj} = 0.039**	**p_{adj} = 0.032**	**p_{adj} = 0.039**	p_{adj} = 0.710

p_{adj} = FDR-corrected p-value.

conflicting: some studies did (Branco et al., 2014; El Mendili et al., 2014) and others did not find a significant correlation (Agosta et al., 2009; Valsasina et al., 2007). On the other hand, we did find a significant correlation between CSA and the ALSFRS-R score for patients with PLS, both for UCSC and individual segments, possibly reflecting a link between functional disability and pure upper motor neuron loss. Importantly, we did find a relationship between the longitudinal measurements of CSA and total ALSFRS-R score, indicating that disease progression is reflected in the cervical spinal cord.

Although we obtained brain and spinal cord measurements from the same image, we could not display a direct relationship between these measurements for the ALS patients. The lack of this direct relationship might be due to the progressive or multifocal pathogenic nature of ALS, possibly leading to different disease effects (of both upper and lower motor neurons) in brain and spinal cord which level out when correlating the two sites. Possible support for this hypothesis is the fact that this relationship was found between spinal cord and the white matter integrity of the CST for PLS and PMA patients. In PLS patients we demonstrated that a thinner spinal cord also correlated with white matter integrity being more affected. The positive correlation for the PLS patients was in line with our expectations and might possibly support UMN involvement in the upper cervical spinal cord. In contrast, the correlation for PMA patients was inverted: more affected white matter integrity implied a thicker spinal cord. This negative correlation for PMA is harder to explain. One might hypothesize the occurrence of a protection mechanism in the upper cervical spinal cord for the PMA patients (preventing them of becoming ALS patients), which needs to be investigated in future research.

The upper cervical spinal cord is a challenging area to image with MRI. Since we have used an MRI protocol initially for the purpose of brain imaging, we analyzed a region at the edge of the FOV. CSA measurements could, therefore, be influenced by intensity drop or gradient nonlinearity (Stroman et al., 2014). However, the MRI images used in our study had a homogeneous signal intensity across the FOV (see Fig. S2 for example images) and were corrected for gradient nonlinearity. Although there still might be measurement errors present in such a small structure as the UCSC, this would affect both patients and controls equally and, therefore, the observed differences in CSA may still be regarded as disease effects.

In this study, we focused on the upper part of the cervical spinal cord that was included on brain MRI. In support of our method, previous research has successfully shown differences in the cervical spinal cord using brain MRI (de Albuquerque et al., 2017). We also revealed disease effects

in the upper cervical spinal cord, but caution is required when interpreting significant results at the level of C4, as analyses of this segment could be applied only to a relatively small group in our study. Investigation of the entire spinal cord would provide a complete overview of atrophy in this important structure. However, as all central motor nerves innervating the upper and lower limbs pass through the upper cervical spinal cord, a correlation with motor deficits could be revealed on the basis of this upper part of the spinal cord. We could not include specific measures for white and grey matter atrophy as the contrast between grey and white matter in the upper cervical spinal cord on our T1-weighted images was not sufficient enough. Future research should include DTI measures and T2- or T2*-weighted MRI to obtain a comprehensive view of grey and white matter damage in the upper cervical spinal cord (Martin et al., 2017; Stroman et al., 2014). Furthermore, test-retesting of the method used in this study and other reliability tests is of importance before upper cervical spinal cord MRI can be used as a biomarker in clinical trials.

In this study, we showed differences between patients and controls in cervical spinal cord MRI, suggesting its potential as diagnostic and longitudinal biomarker in the spectrum of MND.

Disclosure

Appendix A. Supplementary data

Supplementary data to this article can be found online at https://doi.org/10.1016/j.nicl.2019.101984.

References

Agosta, F., Rocca, M.A., Valsasina, P., Sala, S., Caputo, D., Perini, M., Salvi, F., Prelle, A., Filippi, M., 2009. A longitudinal diffusion tensor MRI study of the cervical cord and brain in amyotrophic lateral sclerosis patients. J. Neurol. Neurosurg. Psychiatry 80, 53–55. https://doi.org/10.1136/jnnp.2008.154252.

Agosta, F., Valsasina, P., Riva, N., Copetti, M., Messina, M.J., Prelle, A., Comi, G., Filippi, M., 2012. The cortical signature of amyotrophic lateral sclerosis. PLoS One 7, e42816. https://doi.org/10.1371/journal.pone.0042816.

Bede, P., Hardiman, O., 2018. Longitudinal structural changes in ALS: a three time-point imaging study of white and gray matter degeneration. Amyotroph. Lateral Scler. Front. Degener. 19, 232–241. https://doi.org/10.1080/21678421.2017.1407795.

Bede, P., Bokde, A.L., Byrne, S., Elamin, M., McLaughlin, R.L., Kenna, K., Fagan, A.J., Pender, N., Bradley, D.G., Hardiman, O., 2013. Multiparametric MRI study of ALS stratified for the C9orf72 genotype. Neurology 81, 361–369. https://doi.org/10.1212/WNL.0b013e31829c5eee.

Benjamini, Y., Hochberg, Y., 1995. Controlling the false discovery rate: a practical and powerful approach to multiple testing. J. R. Statiscal Soc. Ser. B 57, 289–300.

Branco, L.M.T., De Albuquerque, M., De Andrade, H.M.T., Bergo, F.P.G., Nucci, A., França, M.C., 2014. Spinal cord atrophy correlates with disease duration and severity in amyotrophic lateral sclerosis. Amyotroph. Lateral Scler. Frontotemp. Degener. 15, 93–97. https://doi.org/10.3109/21678421.2013.852589.

Brooks, B.R., Miller, R.G., Swash, M., Munsat, T.L., 2009. El Escorial revisited: revised criteria for the diagnosis of amyotrophic lateral sclerosis. Amyotroph. Lateral Scler. Other Motor Neuron Disord. 1, 293–299. https://doi.org/10.1080/146608200300079536.

Buchanan, C.R., Pettit, L.D., Storkey, A.J., Abrahams, S., Bastin, M.E., 2015. Reduced structural connectivity within a prefrontal-motor-subcortical network in amyotrophic lateral sclerosis. J. Magn. Reson. Imaging 41, 1342–1352. https://doi.org/10.1002/jmri.24695.

Casserly, C., Seyman, E.E., Alcaide-Leon, P., Guenette, M., Lyons, C., Sankar, S., Svendrovski, A., Baral, S., Oh, J., 2018. Spinal cord atrophy in multiple sclerosis: a systematic review and meta-analysis. J. Neuroimaging 28, 556–586. https://doi.org/10.1111/jon.12553.

Cedarbaum, J.M., Stambler, N., Malta, E., Fuller, C., Hilt, D., Thurmond, B., Nakanishi, A., 1999. The ALSFRS-R: a revised ALS functional rating scale that incorporates assessments of respiratory function. J. Neurol. Sci. 169, 13–21. https://doi.org/10.1016/S0022-510X(99)00210-5.

Chiò, A., Calvo, A., Moglia, C., Mazzini, L., Mora, G., 2011. Phenotypic heterogeneity of amyotrophic lateral sclerosis: a population based study. J. Neurol. Neurosurg. Psychiatry 82, 740–746. https://doi.org/10.1136/jnnp.2010.235952.

Cohen-Adad, J., El Mendili, M.M., Morizot-Koutlidis, R., Lehericy, S., Meininger, V., Blancho, S., Rossignol, S., Benali, H., Pradat, P.F., 2013. Involvement of spinal sensory pathway in ALS and specificity of cord atrophy to lower motor neuron degeneration. Amyotroph. Lateral Scler Front. Degener. 14, 30–38. https://doi.org/10.3109/17482968.2012.701308.

de Albuquerque, M., Branco, L.M., Rezende, T.J., de Andrade, H.M., Nucci, A., Franca Jr., M.C., 2017. Longitudinal evaluation of cerebral and spinal cord damage in amyotrophic lateral sclerosis. Neuroimage Clin. 14, 269–276. https://doi.org/10.1016/j.nicl.2017.01.024.

De Leener, B., Levy, S., Dupont, S.M., Fonov, V.S., Stikov, N., Louis Collins, D., Callot, V., Cohen-Adad, J., 2017. SCT: spinal cord toolbox, an open-source software for processing spinal cord MRI data. Neuroimage 145, 24–43. https://doi.org/10.1016/j.neuroimage.2016.10.009.

de Vries, B.S., Rustemeijer, L.M.M., Bakker, L.A., Schroder, C.D., Veldink, J.H., van den Berg, L.H., Nijboer, T.C.W., van Es, M.A., 2018. Cognitive and behavioural changes in PLS and PMA:challenging the concept of restricted phenotypes. J. Neurol. Neurosurg. Psychiatry. https://doi.org/10.1136/jnnp-2018-318788.

Desikan, R.S., Ségonne, F., Fischl, B., Quinn, B.T., Dickerson, B.C., Blacker, D., Buckner, R.L., Dale, A.M., Maguire, R.P., Hyman, B.T., Albert, M.S., Killiany, R.J., 2006. An automated labeling system for subdividing the human cerebral cortex on MRI scans into gyral based regions of interest. Neuroimage 31, 968–980. https://doi.org/10.1016/j.neuroimage.2006.01.021.

El Mendili, M.-M., Cohen-Adad, J., Pelegrini-Issac, M., Rossignol, S., Morizot-Koutlidis, R., Marchand-Pauvert, V., Iglesias, C., Sangari, S., Katz, R., Lehericy, S., Benali, H., Pradat, P.-F.F., 2014. Multi-parametric spinal cord MRI as potential progression marker in amyotrophic lateral sclerosis. PLoS One 9, 1–7. https://doi.org/10.1371/journal.pone.0095516.

El Mendili, M.-M., Querin, G., Bede, P., Pradat, P.-F., 2019. Spinal cord imaging in amyotrophic lateral sclerosis: historical concepts-novel techniques. Front. Neurol. 10, 350. https://doi.org/10.3389/fneur.2019.00350.

Fischl, B., Salat, D.H., Busa, E., Albert, M., Dieterich, M., Haselgrove, C., van der Kouwe, A., Killiany, R., Kennedy, D., Klaveness, S., Montillo, A., Makris, N., Rosen, B., Dale, A.M., 2002. Whole brain segmentation: automated labeling of neuroanatomical structures in the human brain. Neuron 33, 341–355. https://doi.org/10.1016/S0896-6273(02)00569-X.

Fischl, B., van der Kouwe, A., Destrieux, C., Halgren, E., Ségonne, F., Salat, D.H., Busa, E., Seidman, L.J., Goldstein, J., Kennedy, D., Caviness, V., Makris, N., Rosen, B., Dale, A.M., 2004. Automatically Parcellating the Human Cerebral Cortex. Cereb. Cortex 14, 11–22. https://doi.org/10.1093/cercor/bhg087.

Floeter, M.K., Bageac, D., Danielian, L.E., Braun, L.E., Traynor, B.J., Kwan, J.Y., 2016. Longitudinal imaging in C9orf72 mutation carriers: relationship to phenotype. Neuroimage Clin. 12, 1035–1043. https://doi.org/10.1016/j.nicl.2016.10.014.

Gordon, P.H., Cheng, B., Katz, I.B., Pinto, M., Hays, A.P., Mitsumoto, H., Rowland, L.P., 2006. The natural history of primary lateral sclerosis. Neurology 66, 647–653.

https://doi.org/10.1212/01.wnl.0000200962.94777.71.

Huisman, M.H.B., de Jong, S.W., van Doormaal, P.T.C., Weinreich, S.S., Schelhaas, H.J., van der Kooi, A.J., de Visser, M., Veldink, J.H., van den Berg, L.H., 2011. Population based epidemiology of amyotrophic lateral sclerosis using capture-recapture methodology. J. Neurol. Neurosurg. Psychiatry 82, 1165–1170. https://doi.org/10.1136/jnnp.2011.244939.

Keil, C., Prell, T., Peschel, T., Hartung, V., Dengler, R., Grosskreutz, J., 2012. Longitudinal diffusion tensor imaging in amyotrophic lateral sclerosis. BMC Neurosci. 13. https://doi.org/10.1186/1471-2202-13-141.

Kong, Y., Eippert, F., Beckmann, C.F., Andersson, J., Finsterbusch, J., Büchel, C., Tracey, I., Brooks, J.C.W., Buchel, C., Tracey, I., Brooks, J.C.W., Büchel, C., Tracey, I., Brooks, J.C.W., 2014. Intrinsically organized resting state networks in the human spinal cord. Proc. Natl. Acad. Sci. 111, 18067–18072. https://doi.org/10.1073/pnas.1414293111.

Marini, C., Morbelli, S., Cistaro, A., Campi, C., Caponnetto, C., Bauckneht, M., Bellini, A., Buschiazzo, A., Calamia, I., Beltrametti, M.C., Margotti, S., Fania, P., Poggi, I., Cabona, C., Capitanio, S., Piva, R., Calvo, A., Moglia, C., Canosa, A., Massone, A., Nobili, F., Mancardi, G., Chio, A., Piana, M., Sambuceti, G., 2018. Interplay between spinal cord and cerebral cortex metabolism in amyotrophic lateral sclerosis. Brain 141, 2272–2279. https://doi.org/10.1093/brain/awy152.

Martin, A.R., De Leener, B., Cohen-Adad, J., Cadotte, D.W., Kalsi-Ryan, S., Lange, S.F., Tetreault, L., Nouri, A., Crawley, A., Mikulis, D.J., Ginsberg, H., Fehlings, M.G., 2017. A novel MRI biomarker of spinal cord white matter injury: T2*-weighted white matter to gray matter signal intensity ratio. AJNR Am. J. Neuroradiol. 38, 1266–1273. https://doi.org/10.3174/ajnr.A5162.

Olney, N.T., Bischof, A., Rosen, H., Caverzasi, E., Stern, W.A., Lomen-Hoerth, C., Miller, B.L., Henry, R.G., Papinutto, N., 2018. Measurement of spinal cord atrophy using phase sensitive inversion recovery (PSIR) imaging in motor neuron disease. PLoS One 13, e0208255. https://doi.org/10.1371/journal.pone.0208255.

Querin, G., El Mendili, M.M., Lenglet, T., Delphine, S., Marchand-Pauvert, V., Benali, H., Pradat, P.F., 2017. Spinal cord multi-parametric magnetic resonance imaging for survival prediction in amyotrophic lateral sclerosis. Eur. J. Neurol. 24, 1040–1046. https://doi.org/10.1111/ene.13329.

Querin, G., El Mendili, M.M., Bede, P., Delphine, S., Lenglet, T., Marchand-Pauvert, V., Pradat, P.F., 2018. Multimodal spinal cord MRI offers accurate diagnostic classification in ALS. J. Neurol. Neurosurg. Psychiatry 89, 1220–1221. https://doi.org/10.1136/jnnp-2017-317214.

Rasoanandrianina, H., Grapperon, A.-M., Taso, M., Girard, O.M., Duhamel, G., Guye, M., Ranjeva, J.-P., Attarian, S., Verschueren, A., Callot, V., 2017. Region-specific impairment of the cervical spinal cord (SC) in amyotrophic lateral sclerosis: a preliminary study using SC templates and quantitative MRI (diffusion tensor imaging/inhomogeneous magnetization transfer). NMR Biomed. 30. https://doi.org/10.1002/nbm.3801.

Ravits, J.M., La Spada, A.R., 2009. ALS motor phenotype heterogeneity, focality, and spread: deconstructing motor neuron degeneration. Neurology 73, 805–811. https://doi.org/10.1212/WNL.0b013e3181b6bbbd.

Schmidt, R., Verstraete, E., de Reus, M.A., Veldink, J.H., van den Berg, L.H., van den Heuvel, M.P., 2014. Correlation between structural and functional connectivity impairment in amyotrophic lateral sclerosis. Hum. Brain Mapp. 35, 4386–4395. https://doi.org/10.1002/hbm.22481.

Sperfeld, A.D., Bretschneider, V., Flaith, L., Unrath, A., Hanemann, C.O., Ludolph, A.C., Kassubek, J., 2005. MR-pathologic comparison of the upper spinal cord in different motor neuron diseases. Eur. Neurol. 53, 74–77. https://doi.org/10.1159/000084650.

Stroman, P.W., Wheeler-Kingshott, C., Bacon, M., Schwab, J.M., Bosma, R., Brooks, J., Cadotte, D., Carlstedt, T., Ciccarelli, O., Cohen-Adad, J., Curt, A., Evangelou, N., Fehlings, M.G., Filippi, M., Kelley, B.J., Kollias, S., Mackay, A., Porro, C.a, Smith, S., Strittmatter, S.M., Summers, P., Tracey, I., 2014. The current state-of-the-art of spinal cord imaging: methods. Neuroimage 84, 1070–1081. https://doi.org/10.1016/j.neuroimage.2013.04.124.

Valsasina, P., Agosta, F., Benedetti, B., Caputo, D., Perini, M., Salvi, F., Prelle, A., Filippi, M., 2007. Diffusion anisotropy of the cervical cord is strictly associated with disability in amyotrophic lateral sclerosis. J. Neurol. Neurosurg. Psychiatry 78, 480–484. https://doi.org/10.1136/jnnp.2006.100032.

Van Rheenen, W., Van Blitterswijk, M., Huisman, M.H.B., Vlam, L., Van Doormaal, P.T.C., Seelen, M., Medic, J., Dooijes, D., De Visser, M., Van Der Kooi, A.J., Raaphorst, J., Schelhaas, H.J., Van Der Pol, W.L., Veldink, J.H., Van Den Berg, L.H., 2012. Hexanucleotide repeat expansions in C9ORF72 in the spectrum of motor neuron diseases. Neurology 79, 878–882. https://doi.org/10.1212/WNL.0b013e3182661d14.

Verstraete, E., Veldink, J.H., Mandl, R.C.W., van den Berg, L.H., van den Heuvel, M.P., 2011. Impaired structural motor connectome in amyotrophic lateral sclerosis. PLoS One 6. https://doi.org/10.1371/journal.pone.0024239.

Verstraete, E., Veldink, J.H., van den Berg, L.H., Van den Heuvel, M.P., 2014. Structural brain network imaging shows expanding disconnection of the motor system in amyotrophic lateral sclerosis. Hum. Brain Mapp. 35, 1351–1361. https://doi.org/10.1002/hbm.22258.

Visser, J., van den Berg-Vos, R.M., Franssen, H., van den Berg, L.H., Wokke, J.H., de Jong, J.M.V., Holman, R., de Haan, R.J., de Visser, M., 2007. Disease course and prognostic factors of progressive muscular atrophy. Arch. Neurol. 64, 522–528. https://doi.org/10.1001/archneur.64.4.522.

Walhout, R., Westeneng, H.-J., Verstraete, E., Hendrikse, J., Veldink, J.H., van den Heuvel, M.P., van den Berg, L.H., 2015. Cortical thickness in ALS: towards a marker for upper motor neuron involvement. J. Neurol. Neurosurg. Psychiatry 86, 288–294. https://doi.org/10.1136/jnnp-2013-306839.

Wang, Yan, Liu, L., Ma, L., Huang, X., Lou, X., Wang, Yulin, Wu, N., Liu, T., Guo, X., 2014. Preliminary study on cervical spinal cord in patients with amyotrophic lateral

sclerosis using MR diffusion tensor imaging. Acad. Radiol. 21, 590–596. https://doi.org/10.1016/j.acra.2014.01.014.

Westeneng, H.-J., Verstraete, E., Walhout, R., Schmidt, R., Hendrikse, J., Veldink, J.H., van den Heuvel, M.P., van den Berg, L.H., 2015. Subcortical structures in amyotrophic lateral sclerosis. Neurobiol. Aging 36, 1075–1082. https://doi.org/10.1016/j.neurobiolaging.2014.09.002.

Westeneng, H.-J., Walhout, R., Straathof, M., Schmidt, R., Hendrikse, J., Veldink, J.H., Van Den Heuvel, M.P., Van Den Berg, L.H., 2016. Widespread structural brain involvement in ALS is not limited to the C9orf72 repeat expansion. J. Neurol. Neurosurg. Psychiatry 87, 1354–1360. https://doi.org/10.1136/jnnp-2016-313959.

Westeneng, H.-J., Debray, T.P.A., Visser, A.E., van Eijk, R.P.A., Rooney, J.P.K., Calvo, A., Martin, S., McDermott, C.J., Thompson, A.G., Pinto, S., Kobeleva, X., Rosenbohm, A., Stubendorff, B., Sommer, H., Middelkoop, B.M., Dekker, A.M., van Vugt, J.J.F.A., van Rheenen, W., Vajda, A., Heverin, M., Kazoka, M., Hollinger, H., Gromicho, M., Körner, S., Ringer, T.M., Rödiger, A., Gunkel, A., Shaw, C.E., Bredenoord, A.L., van Es, M.A., Corcia, P., Couratier, P., Weber, M., Grosskreutz, J., Ludolph, A.C., Petri, S., de Carvalho, M., Van Damme, P., Talbot, K., Turner, M.R., Shaw, P.J., Al-Chalabi, A., Chiò, A., Hardiman, O., Moons, K.G.M., Veldink, J.H., van den Berg, L.H., 2018. Prognosis for patients with amyotrophic lateral sclerosis: development and validation of a personalised prediction model. Lancet Neurol. 17, 423–433. https://doi.org/10.1016/s1474-4422(18)30089-9.

Yendiki, A., Panneck, P., Srinivasan, P., Stevens, A., Zöllei, L., Augustinack, J., Wang, R., Salat, D., Ehrlich, S., Behrens, T., Jbabdi, S., Gollub, R., Fschl, B., 2011. Automated probabilistic reconstruction of white-matter pathways in health and disease using an atlas of the underlying anatomy. Front. Neuroinform. 5. https://doi.org/10.3389/fninf.2011.00023.